Colloids and Surfaces A: Physicochem. Eng. Aspects 519 (2017) 231–237

Contents lists available at ScienceDirect

Colloids and Surfaces A: Physicochemical and Engineering Aspects

journal homepage: www.elsevier.com/locate/colsurfa

Grafted semiconductors on PE-films leading to bacterial inactivation: Synthesis, characterization and mechanism

A. Camarasa Mena[a], S. Rtimi[a,*], C. Pulgarin[a,*], J.-C. Lavanchy[b], J. Kiwi[a]

[a] Ecole Polytechnique Fédérale de Lausanne, EPFL-SB-ISIC-GPAO, Station 6, CH-1015, Lausanne, Switzerland
[b] Lausanne University, IMG, Mineral analysis center, Bat Anthropole, CH-1015 Lausanne, Switzerland

HIGHLIGHTS

- The bacterial inactivation by colloidal prepared FeOx-TiO_2-PE films is reported.
- The surface potential decreased during bacterial inactivation due to cell-wall damage.
- The FeOx-TiO_2-PE films released ppm of Fe not affecting the film performance.
- The hydrophilicity of films was observed to increase during bacterial inactivation.

GRAPHICAL ABSTRACT

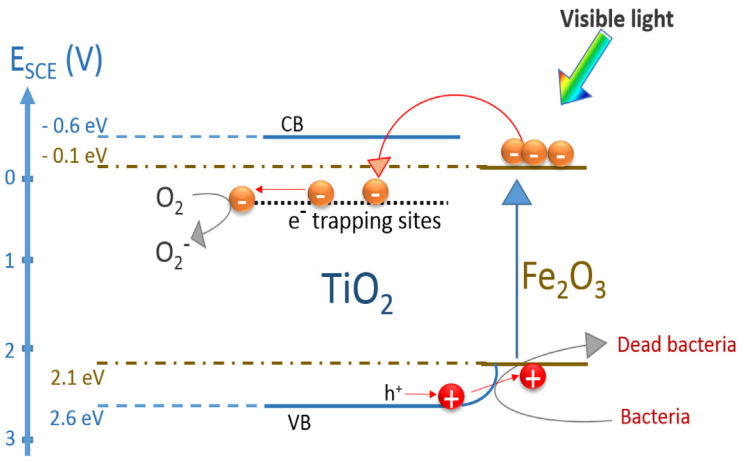

ARTICLE INFO

Article history:
Received 13 April 2016
Received in revised form 15 July 2016
Accepted 16 July 2016
Available online 25 July 2016

Keywords:
Semiconductor films
Colloidal preparations
Grafting of nanoparticles
Bacterial inactivation
IFCT

ABSTRACT

This study reports the colloidal preparation FeOx, TiO_2 and FeOx-TiO_2 grafted on polyethylene (PE) films leading to bacterial inactivation. A fast bacterial inactivation was attained by the FeOx-TiO_2 compared to the FeOx-PE film due to the interfacial charge transfer (IFCT) FeOx to the lower-lying TiO_2 trapped states. A pH-decrease was observed during bacterial inactivation due to the formation of carboxylic acids on the grafted films and the recovery to the initial pH ~7 after elimination of the intermediates was followed quantitatively during bacterial inactivation. The potential on the TiO_2-PE, FeOx-PE and FeOx-TiO_2-PE film surfaces decreased during the bacterial inactivation concomitant with the loss of the cell wall permeability. Different mechanisms for the photo-induced *E. coli* inactivation for random nanoparticulate FeOx-PE and FeOx-TiO_2-PE films are suggested based on the experimental observations reported in this study. During the inactivation of *E. coli*, the Fe-ions were seen to leach out in amounts $\leq$ 0.45 ppm. This is within the EU sanitary allowed limits for industrial/drinking water. The wettability of the films was followed by contact angle measurements (CA) within the time of bacterial inactivation. By diffuse reflectance spectroscopy (DRS), the conversion of the Fe(III)-oxide to Fe(II)-oxide is reported during film recycling. The change in the Fe-oxidation states within the bacterial inactivation was further confirmed by X-ray photoelectron spectroscopy (XPS).

http://dx.doi.org/10.1016/j.colsurfa.2016.07.034
0927-7757/

1. Introduction

Bacterial inactivation materials/films have widely used TiO_2 and Fe-oxides under sunlight irradiation leading to highly oxidative radicals [1–7]. TiO_2 absorbs only 4–5% of the incident solar radiation with an absorption edge at ~390 nm. A method to increase the visible light absorption is to couple TiO_2 with narrow band-gap iron-oxide(s) semiconductor [8,9]. Fe-oxides have also been used as TiO_2 dopants due to its small band gap (~2.2 eV) for α-Fe_2O_3, low cost and non-toxicity [10,11].

Studies with FeOx and the FeOx-TiO_2 binary oxide have shown to induce an accelerated degradation of arsenite [12], phenol [13], 4-chlorophenol [14] and humic acids [15] under visible light. More recently, our laboratory has reported FeOx-PE [16] and FeOx-TiO_2-PE films [17] prepared by direct magnetron current sputtering presenting antibacterial properties. In this study we address the colloidal preparation of TiO_2-PE, FeOx-PE and FeOx-TiO_2 films prepared by a simple, low temperature approach and their subsequent grafting on PE. Iron oxide nanoparticles (NP's) are of considerable interest due to their wide applications in fields such as magnetic storage, medicine, chemical industries, catalytic materials and water purification. Synthesis of Fe_2O_3/FeO have been carried out by precipitation, sol-gel, hydrothermal, dry vapor deposition, surfactant mediation, micro-emulsion, electro-deposition and sonochemical methods [9,18,19]. We have selected polyethylene (PE) as the substrate for the selected oxides for its stability, lack of oxidation when exposed to air and/or sunlight and its low cost. Immobilized Fe-catalysts avoid the problem of separation and filtration of the iron oxides when suspensions are used at the end of the pollutant abatement process. For this reason our laboratory has reported the degradation of pollutants on Fe-supported on PE-maleic anhydride films [20] and also on Fe immobilized on sulfonic Nafion exchange membranes [21]. The bacterial inactivation kinetics on colloidal FeOx-TiO_2-PE with respect to FeOx-PE and TiO_2-PE [22,23] is investigated in this study addressing film surface properties.

The novelty of this study consists in the presentation: a) of an innovative colloidal preparation of oxides and their deposition on non-thermal resistant films like PE. The deposition of oxides on thermally resistant surfaces reported until now required temperatures of few hundred degrees necessary to anneal the oxides on the support [10,18]. A procedure is also presented to graft the selected oxides on PE at temperatures within the thermal resistance of PE (<96 °C), b) the evaluation o;1;f the *E. coli* inactivation kinetics on the FeOxTiO_2-coated films c) a mechanistic outline for the photo-induced charge from FeOx to TiO_2, based on X-ray photo-electron spectroscopy (XPS) providing a proof for the *redox* process taking place during bacterial inactivation and d) the film properties characterized by several complementary techniques such as: X-ray fluorescence (XRF), diffuse reflection spectroscopy (DRS), contact angle (CA), surface potential changes and X-ray photoelectron spectroscopy (XPS).

2. Experimental

2.1. Preparation of TiO_2, FeOx and FeOx-TiO_2 colloids and PE functionalization and determination of the oxide loading on PE by XRF

Colloidal solutions of $FeCl_3$ and TiO_2 Degussa P25 were prepared using the concentration of $FeCl_3$ (100 mg/L) and TiO_2 (5 g/L) to photo-corrode the PE. The photo-corrosion was carried out under UV irradiation for 15 h. For this purpose BLB lamp Philips TLD-15W/08 SLV was used providing monochromatic 366 nm light with an integral output of 4.3 mW/cm^2. The photo-corrosion step introduces oxidative chelating sites to bind the oxides (TiO_2 and/or FeOx). After the UV-irradiation, the films were sonicated in aqueous solution for 10 min to remove loose bound oxide particles, washed and dried and dried for 10 min at 80 °C. Afterwards, the PE was functionalized in air by contacting different concentrations of FeOx and/or TiO_2 for 2 h. This deposition was made without further UV-photo-assisted illumination. This operation was repeated twice and the loaded films were dried at 60 °C.

Table 1
Loading of polyethylene (PE) by FeOx, TiO_2 and FeOx-TiO_2 determined by X-ray fluorescence (XRF).

	Fe wt%/wt PE	Ti wt%/wt PE
FeOx (25 mg/L)	0.076	–
FeOx (100 mg/L)	0.261	–
FeOx (150 mg/L)	0.240	–
TiO_2 (200 mg/L)	–	0.788
TiO_2 (250 mg/L)	–	0.624
FeOx(100 mg/L)/TiO_2 (250 mg/L)	0.075	0.655
FeOx(25 mg/L)/TiO_2 (200 mg/L)	0.063	0.702

The amounts of Fe and Ti on PE were determined by X-ray fluorescence spectroscopy (XRF) in a PANalytical PW2400 spectrometer and are shown in Table 1.

The polyethylene (PE) film used consisted of highly branched low crystalline semi-transparent film with the formula H(CH_2-CH_2)H. The (LDPE) 0.1 mm thick was obtained from Goodfellow (UK, ET3112019) had a density of 0.92 g/cm^3.

2.2. E. coli inactivation on FeOx-TiO_2-PE films, irradiation procedures and determination of the Fe leached out from the films during bacterial inactivation

The samples of *Escherichia coli* (*E. coli K12*) on 2 cm by 2 cm FeOx-PE, TiO_2-PE and FeOx-TiO_2-PE were placed into a glass Petri dish and irradiated in the cavity of Sunlight simulated cavity set at one half of the maximum sunlight intensity (50 mW/cm^2) emitting in the range 310–800 nm. The 100 μL culture aliquots with an initial concentration of ~10^6 colony forming units (CFU mL^{-1}) in NaCl/KCl (pH 7) were placed on coated PE. After preselected irradiation times, the fabric was transferred into a sterile Eppendorf tube containing 900 μL autoclaved NaCl/KCl saline solution. This solution was subsequently mixed thoroughly using a Vortex. Serial dilutions were made in NaCl/KCl solution. Samples of 100-μL were pipetted onto a nutrient agar plate and then spread over the surface of the plate using standard plate method. Agar plates were incubated lid down, at 37 °C for 24 h before counting. Three independent assays were carried out for each sputtered sample. The coated and uncoated (control) films were kept in a sterile oven at 60 °C to avoid contamination prior to the bacterial test. Films irradiation was carried out on Petri dishes provided with a lid to prevent the bacterial suspension evaporation. The agar was purchased from Merck GmbH, Microbiology division KGaA under the catalogue N° 1.05463.0500. The CFU statistical analysis of the bacteria inactivation data was performed calculating the standard deviation values.

The irradiation of the samples was carried out in the cavity of a sunlight simulator from Atlas Material Testing Solutions (Harkingen, Switzerland) tuned at a light dose of 50 mW/cm^2 provided for with a filter blocking the light <310 nm.

Ferrozine was used to evaluate the total iron concentration leaching out during the bacterial inactivation following the optical absorption 562 nm of the Fe(II), in a buffered solution [24]. The Fe(III) species was determined by difference adding hydroxylamine

* Corresponding authors.
E-mail address: sami.rtimi@epfl.ch (S. Rtimi).

hydrochloride to reduce the Fe(III) to Fe(II)-species, its absorbance peak taken after 3 min again at 562 nm. The addition of the two Fe-species is reported in this study during the bacterial inactivation period.

2.3. Diffuse reflectance spectroscopy (DRS), contact angle (CA) and surface potential changes during bacterial inactivation on TiO_2, FeOx and FeOx-TiO_2-PE films

Diffuse reflectance spectroscopy (DRS) was carried out in a Perkin Elmer Lambda 900 UV-VIS-NIR spectrometer provided for with a PELA-1000 accessory within the wavelength range of 200–800 nm and a resolution of 1 nm. The absorption of the samples was plotted in Kubelka-Munk (KM/S units) vs wavelength.

The CA of the films were determined by the sessile drop method on a DataPhysics OCA 35 unit. Drop volumes of 0.5 microliter were chosen in all experiments to avoid shape alteration due to gravitational forces and to diminish the evaporation effects. The measurements were performed at room temperature (65% controlled humidity). The drop image was registered in a CCD camera (1280 × 960 pixels) attached to a microscope and processed by way of software image analysis to estimate the contact angle.

The local pH and surface potential changes within the bacterial inactivation were followed by the mean of a Jenco 6230 N (pH/mV/Temp meter) provided for with a hand held microprocessor in splash proof case with 3 points calibration. The data was monitored via RS-232-C IBM compatible communication interface and BNC, pH/ORP connector with 8-pin DIN ATC connector.

2.4. The X-ray photoelectron spectroscopy (XPS) of the films during bacterial inactivation

The X-ray photoelectron spectroscopy (XPS) of the films was carried out using an AXIS NOVA photoelectron spectrometer (Kratos Analytical, Manchester, UK) provided for with a monochromatic AlK_a ($h\nu = 1486.6$ eV) anode. The carbon C1 s line with position at 284.6 eV was used as a reference to correct the charging effect. The surface atomic concentration was determined from peak areas using the known sensitivity factors for each element [25]. Spectrum background was subtracted according to Noggier et al., [26]. Deconvolution of the XPS peaks was carried out taking into consideration the Shirley background correction and Gaussian-Lorentzian peak shape with a G-L ratio of 30. The XPS spectral peaks were deconvoluted with a CasaXPS-Vision 2, Kratos Analytical UK.

3. Results an discussions

3.1. Bacterial inactivation on PE-coated films and amount of Fe-eluted during the bacterial inactivation process

Fig. 1 shows the bacterial inactivation under low intensity simulated solar light on FeOx-TiO_2-PE films within 90 min, on FeOx-PE within 120 min and finally on TiO_2-PE at 240 min. Therefore, semiconductors with a different make up under light or their combinations led to different bacterial inactivation times. The mechanism of FeOx charge photo-generation will not be described in this study since it has been recently reported in our laboratory [16]. Also the TiO_2-PE mediated bacterial inactivation has been reported widely in the open literature [1–3,18]. Below Eqs. (1–6) outline the photo-induced bacterial inactivation due to TiO_2-PE shown in Fig. 1, trace 2:

$$\text{Bacteria} + [TiO_2\text{-PE}] + \text{light} \rightarrow [TiO_2{*}\text{-PE}]\text{Bacteria} \rightarrow [\text{Bacteria}^+ \cdots TiO_2(cbe^-)\text{-PE}] \quad (1)$$

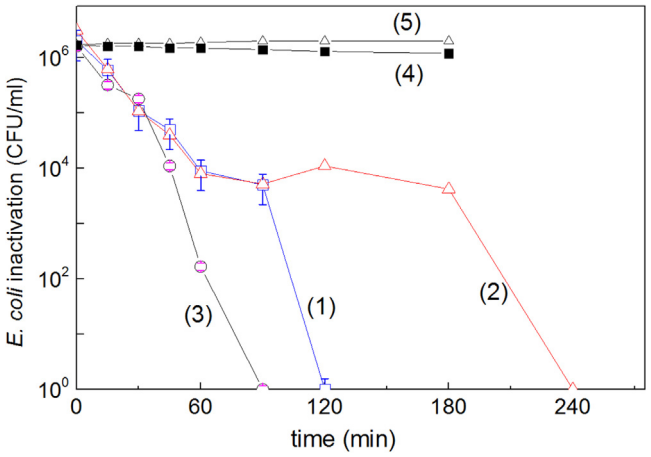

Fig. 1. *E. coli* inactivation (CFU/ml) on PE-films coated with (1) FeOx and (2) TiO_2 and (3) FeOx-TiO_2 under low intensity solar simulated light (50 mW/cm^2).

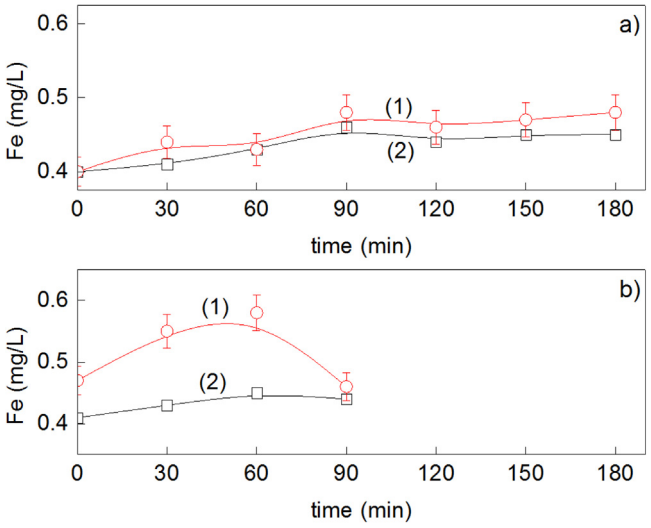

Fig. 2. a Tarace (1) presents the Fe(mg/L) leached out from a solution FeOx-PE under sunlight with a Fe loading of 0.261 wt% / wt PE in the presence of 10^6 CFU/ml. Trace 2 presents the Fe-leaching from similar films but in the absence of *E. coli.* (b) Tbrace (1) presents the Fe(mg/L) leached out from a solution FeOx-TiO_2-PE under sunlight with a Fe loading of 0.788 wt %/wt PE in the presence of 10^6 CFU/ml. Trace 2 presents the Fe-leaching from similar films but in the absence of *E. coli.*.

$$TiO_2(cbe\text{-})\text{-PE} + O_2 + H^+ \rightarrow HO_2^{\circ}\ E_0 - 0.05\text{NHE}[27] \quad (2)$$

$$TiO_2(cbe\text{-})\text{-PE} + O_{2ads} \rightarrow O_2^{\circ -}{}_{ads}\ E_0 - 0.16\text{NHE}[27] \quad (3)$$

$$TiO_2(vbh^+)\text{-PE} + OH^-{}_{ads} \rightarrow OH^{\circ}\ E_0 - 1.90\text{NHE}[9] \quad (4)$$

$$TiO_2(vbh^+)\text{-PE} + H_2O_{ads} \rightarrow OH^{\circ}{}_{ads} + H^+ \quad (5)$$

$$O_2^{\circ -} + H^+ \Leftrightarrow HO_2^{\circ}\ pK_a 4.8 \quad (6)$$

In reaction (2), the HO_2° radical generated under light is stable at pH <4.8, but above this pH more than 50% (as noted in Eq. (3)) in the form of $O_2^{\circ -}$ as noted in reaction (6).

Fig. 1, trace 3 presents the bacterial inactivation mediated by FeOx-TiO_2-PE. This later film is seen to accelerate the bacterial inactivation kinetics respect to the TiO_2 and FeOx coated PE-films. Therefore, the interaction going on between the random coated FeOx and TiO_2 on the PE film surface accelerates the observed bacterial inactivation. A mechanism will be suggested at a later stage in Section 3.4 consistent with the observed results.

Fig. 2 presents the Fe-leaching by way of ferrozine (see experimental section) during bacterial inactivation. Fig. 2a shows the Fe-leaching for FeOx-PE films. In this case, the electrostatic attraction between the negative *E. coli* envelope and the positively charged FeOx (I.E.P. ~9) film plays a role. This interaction occurs in the pH range 6–7 tolerable by the bacterial cells. For this reason, Fig. 2a, trace (2) shows a low Fe-leaching within the 120 min bacterial inactivation time. Fig. 2b presents the same trend for the Fe-leaching from FeOx-TiO_2 films within the 90 min bacterial inactivation time. In both cases, the Fe-leached is below the limit of 1–2 mg/L Fe set for drinking water [28].

3.2. UV–vis spectroscopic properties and surface wettability of coated-PE films

Fig. 3a shows the DRS spectra of TiO_2 and FeOx in Kubelka-Munk units. The spectrum of FeOx shown in Fig. 3a suggests that the main component is hematite showing an absorption similar to the one presented in Fig. 3 [29]. The absorption spectrum between 250 and 450 nm in Fig. 2a is attributed to Fe_2O_3 and to amorphous/anatase TiO_2 with bigger particle sizes. The higher amplitude of the TiO_2 spectrum in Fig. 3a was due to the larger TiO_2 particles compared to their FeOx (Fe_2O_3) counterparts. Both spectra have been extensively reported as a function of the film thickness and particulate grain size [9,18]. Fig. 3b shows that the spectra of FeOx-TiO_2-PE after several bacterial inactivation cycles. The FeOx-TiO_2-films spectral absorption presents only a minor variation providing the proof for the stability of the coating described in Section 2.1. Due to the low temperature used during the film preparation, the incorporation of FOx in the TiO_2 lattice seems not to be possible. But the random distribution of the FeOx and TiO_2 particles in the colloidal coated film may involve charge transfer between these two particles. This will be discussed below in Section 3.4 in relation to the photo-induced interfacial charge transfer (IFCT) between FeOx and TiO_2.

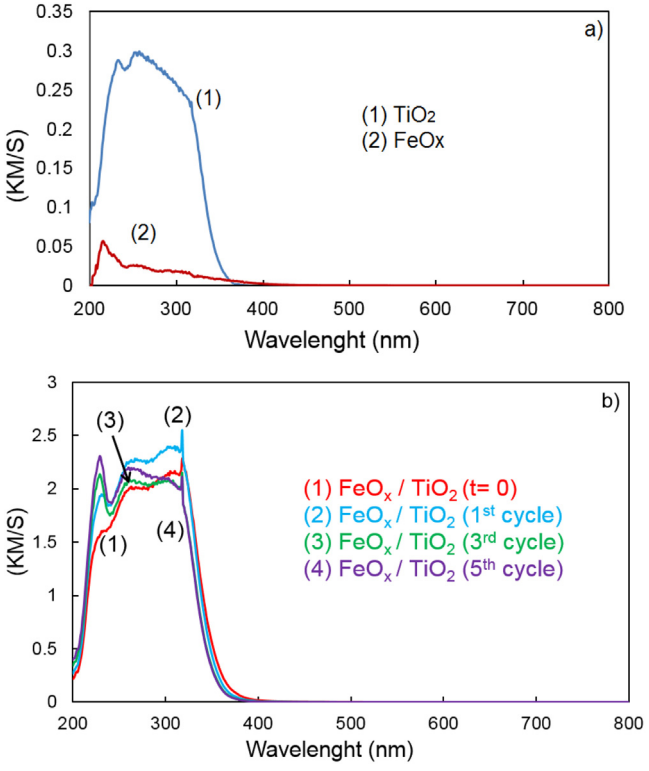

Fig. 3. a Daiffuse reflectance spectroscopy (DRS) of TiO_2 and FeOx coated PE-films, Fig. 3b. Diffuse reflectance spectroscopy (DRS) of FeOx-TiO_2 coated PE up to the fifth recycling after bacterial inactivation.

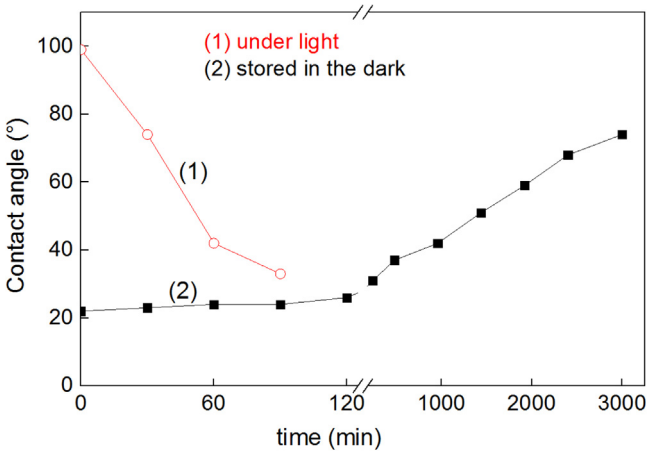

Fig. 4. Trace 1: Contact angle (CA) kinetics during the hydrophobic-hydrophilic kinetics of the FeOx-TiO_2-PE film under low intensity solar light (50 mW/cm^2), Trace 2: reverse hydrophilic-hydrophobic back kinetics after bacterial inactivation (samples kept in the dark).

The hydrophobic to hydrophilic transformation for the FeOx-TiO_2-PE films under low intensity sunlight is shown next in Fig. 4. The hydrophobic FeOx-TiO_2-PE film at time zero presents and angle of ~100° decreasing under light within the time of bacterial inactivation to ~32° (90 min) [30]. The recovery in the dark towards an increased hydrophobicity is shown in Fig. 3b beginning around 22° and proceeding slowly in the time scale up to 3000 min. The fact that the recovery in the dark starts at 22° and not 32° was due to the 6 h elapsed when taking the last point in Fig. 4, trace 1 before registering the zero point reported in Fig. 4, trace 2. The FeOx-TiO_2-PE film increase in hydrophilicity continues after 90 min irradiation approaching the super-hydrophilicity range [31]. Recently, Amal et al., have reported reversibly photo-switching within cyclic light-dark cycles mediated by the Ag-particles [32]. The hydrophilic or hydrophobic character of the bacterial cell-wall envelope is important for the adhesion of *E. coli* an event preceding inactivation. *E. coli* has been shown to present preferential adhesion to hydrophilic surfaces [33].

3.3. X-ray photoelectron spectroscopy (XPS) micro-potential analysis and shift in the local pH during bacterial inactivation

Fig. 5a/a shows the deconvolution of the Fe- XPS peaks of the FeOx-TiO_2-PE film before bacterial inactivation. The Fe-ion, Fe_2O_3, FeOOH and FeOH peaks have been assigned according to Wagner [25] and the data corrected for electrostatic charging according to Shirley [34]. After bacterial inactivation, new Fe-species and Fe^{2+}-satellite peaks appear as seen in Fig. 5a/b. A significant change in the binding energy if FeOH peak from 713.0 eV to 714.2 eV is seen after the bacterial inactivation. *Redox* catalysis associated with FeOx therefore plays a significant role during bacterial inactivation. This was also confirmed by the appearance of significantly shifted Fe^{2+}−satellite peaks concomitant with bacteria inactivation. The Fe_3O_4 after bacterial inactivation appears probably at the expense of a reduction of the Fe^{2+}-species during the bacterial inactivation in Fig. 5a/a.

Further evidence for *redox* catalysis by XPS is shown in Fig. 5b/a. The Ti2p doublet peak of FeOx-TiO_2-PE film was found at 457.75 eV before bacterial inactivation and is shifted to the 458.21 eV after the bacterial inactivation.

The changes in pH and surface potential were followed within the time of bacterial inactivation and the results are presented

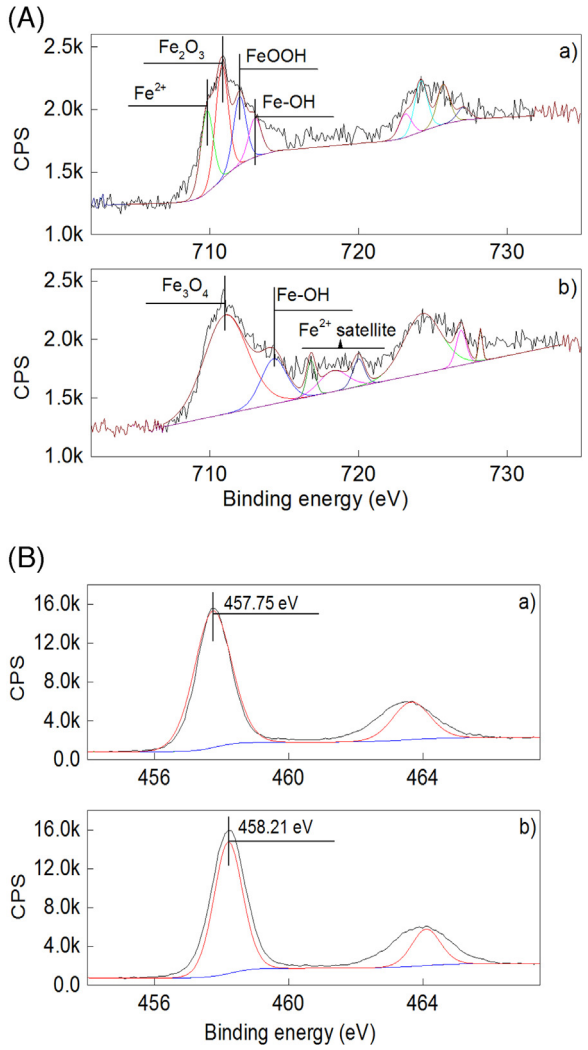

Fig. 5. a XaPS deconvolution of the Fe2p doublet on FeOx-TiO_2-PE films: (a) before and (b) after bacterial inactivation under solar simulated light (50 mW/cm^2). (b) XbPS deconvolution of Ti2p doublet on FeOx-TiO_2-PE: (a) before and (b) after bacterial inactivation under solar simulated light (50 mW/cm^2).

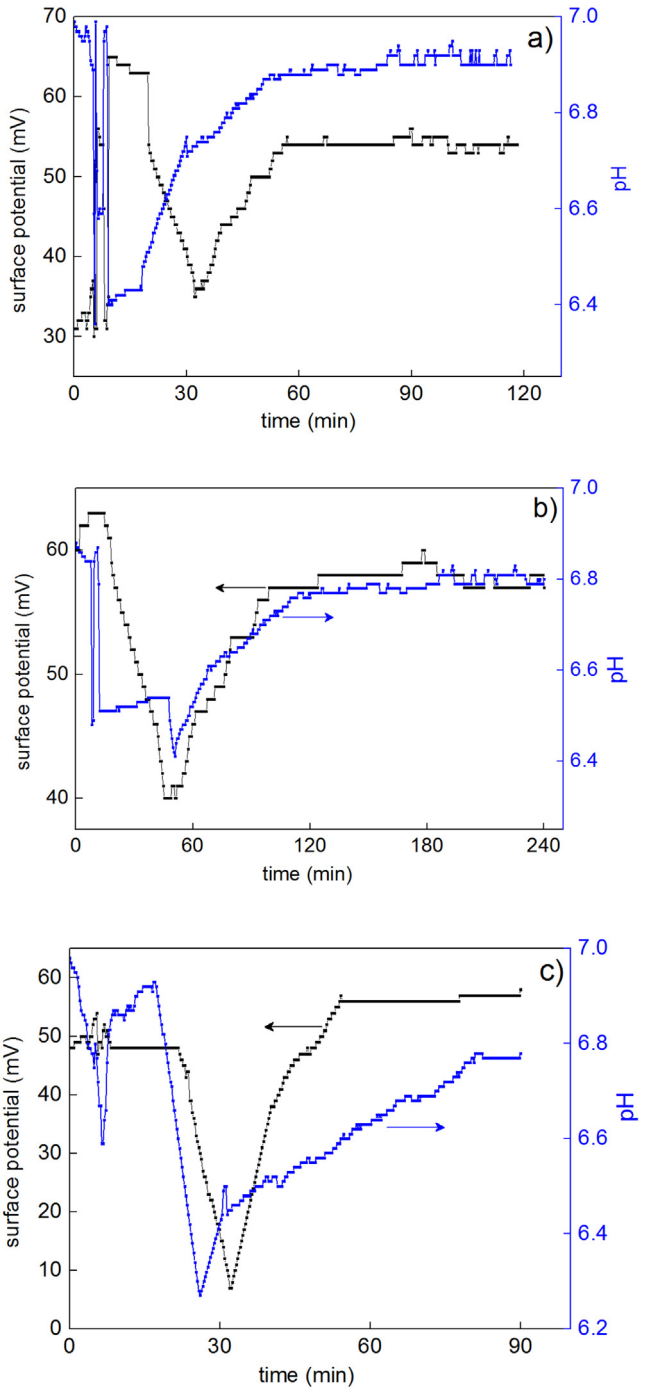

Fig. 6. a Saurface pH and potential changes on FeOx-PE films during bacterial inactivation under solar simulated light (50 mW/cm^2). (b) Sburface pH and potential changes on TiO_2-PE films during bacterial inactivation under solar simulated light (50 mW/cm^2). (c) Scurface pH and potential changes on FeOx-TiO_2-PE films during bacterial inactivation under solar simulated light (50 mW/cm^2).

in Fig. 6a and b. This allows to gain further insight into the changes on the surface of the film during bacterial inactivation. A mechanism of bacterial inactivation involves the generation of intermediate species by TiO_2 and FeOx semiconductors under band-gap-irradiation [18,35].

Fig. 6a presents the surface pH-shift at the FeOx-PE interface under low intensity solar light irradiation. A pH-decrease between 7.0 and pH 6.5 was observed within 30 min. The decrease in pH-shift is equivalent to a fourfold increase in the concentrations of [H^+]. The pH decrease is due to short chain carboxylic acids generated in solution during the bacterial inactivation. These carboxylic acids have pK_a values around ~3 [5]. After 30 min, the pH recovers up to ~6.7 due to the elimination of short carboxylic acids through mineralization of the carboxylic acids to CO_2. This is the final step in the bacterial mineralization known as the typical photo-Kolbe CO_2 elimination reaction [36] and is shown below in Eq. (7).

$$\text{RCOO-} + \text{FeOx-TiO}_2\text{-PE} + h\nu \rightarrow R^{\circ} + CO_2 \quad (7)$$

Fig. 6b and c follow the same trend for TiO_2-PE and for the FeOx-TiO_2-PE films respectively. A steeper pH decrease for the pH-values was observed within the bacterial inactivation followed by a recover to pH 6.8.

Fig. 6a shows that the interface potential decrease for FeOx-PE decreases from 70 to 30 mV during the first 5 min during the bacterial inactivation. This decrease in voltage at the film-surface is concomitant to the cell wall permeability. The voltage decrease is due to the loss/damage of the cell wall barrier regulating the ions exchange in and out of the cell cytoplasm [37]. As a consequence the bacteria loses K, Na, Mg-ions and other essential ions, diffuse faster out of the cell wall envelope [38,39]. The surface potential recovery after 30 min in Fig. 6a reflects the recovery of the FeOx-TiO_2-PE initial potential once the film recovers its initial microstructure after

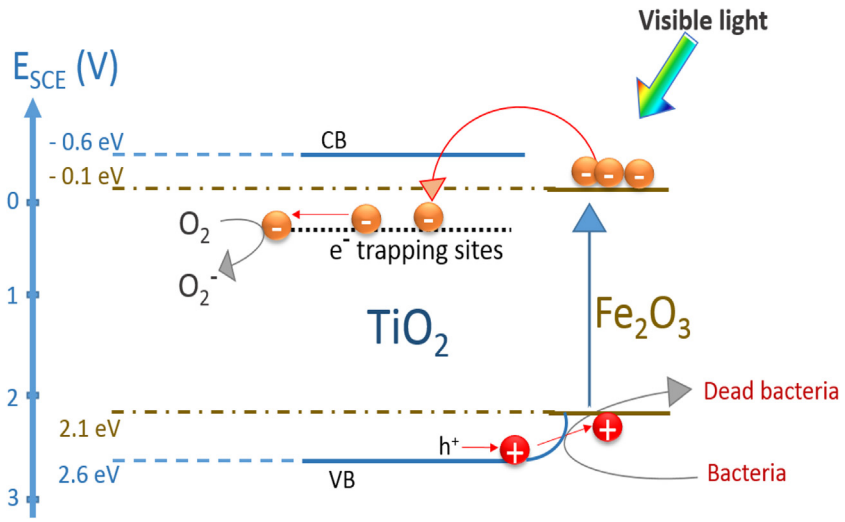

Fig. 7. Interfacial charge transfer (IFCT) electron transfer between FeOx and low-lying TiO_2 trapped states.

bacterial inactivation. Fig. 6b shows a surface potential loss and recovery similar as the one reported in Fig. 6a but for TiO_2-PE films. But Fig. 6c shows a steeper surface potential drop of ~5 mV for the FeOx-TiO_2-PE films. This is possibly due to the faster bacterial inactivation kinetics induced by FeOx-TiO_2-PE films seen in Fig. 1.

3.4. Suggested mechanism of bacterial inactivation by FeOx-TiO_2-PE films

Fig. 1 showed that FeOx-TiO_2-PE films led to bacterial inactivation within 90 min. This kinetic is faster compared to the 120 min required by FeOx-PE films. Fig. 7 suggests a mechanism for the electron transfer from FeOx into lower lying TiO_2 trapping states. Leytner et al., [40] by time-resolved photo-acoustic spectroscopy (TRPAS) identified the electron trapping sites in anatase positioned at ~0.8 eV below the anatase cb. Gray et al., [41] used electron paramagnetic resonance (EPR) spectroscopy to report anatase trapping sites located ~0.5–0.8 eV below the anatase cb. FeOx (mainly Fe_2O_3) powders have been reported to present cb located 0.4-0.6 eV below anatase [9,18,28]. The mechanism of the bacterial inactivation mediated by TiO_2-PE was outlined above in Eqs. (1–7). The intervention of FeOx injecting e^- into TiO_2 is suggested in Eqs. (3–13):

$$\text{FeOx} + \text{Vislight} \rightarrow \text{FeOx(e-)} + \text{FeOx(h+)} \quad (8)$$

$$\text{FeOx(e-)} + \text{TiO}_2 \rightarrow \text{FeOx} + \text{TiO}_2(\text{e-}_{\text{trappe site}}) \quad (9)$$

$$\text{FeOx(e-)} + \text{O}_2 \rightarrow \text{FeOx} + \text{O}_2^- \quad (10)$$

$$\text{O}_2^{-\circ} + \text{H}^+ \rightarrow \text{HO}_2^\circ \rightarrow \text{ROS(reactiveoxygenspecies)} \quad (11)$$

$$\text{TiO}_2(\text{e-}_{\text{trappedsite}}) + \text{O}_2 \rightarrow \text{TiO}_2 + \text{O}_2^- \rightarrow \text{ROSspecies} \quad (12)$$

$$\text{TiO}_2(\text{h+}) + \text{bacteria} \rightarrow \text{CO}_2 + \text{H}_2\text{O} + \text{inorganic/organicresidues} \quad (13)$$

A mechanism of reaction between FeOx-TiO_2-PE and bacteria under visible light is suggested hereafter in Eq. (14):

$$\text{Bacteria} + [\text{FeOx-TiO}_2\text{-PE}] + \text{Vislight} \rightarrow [\text{bacteria}\cdots\text{Fe}*\text{Ox-TiO}_2]\text{PE} \rightarrow [\text{bacteria}*\ldots\text{.FeOx-TiO}_2]\text{PE} \rightarrow [\text{bacteria} + \cdots\text{FeOx-TiO}_2\text{(e-)}]\text{PE}. \quad (14)$$

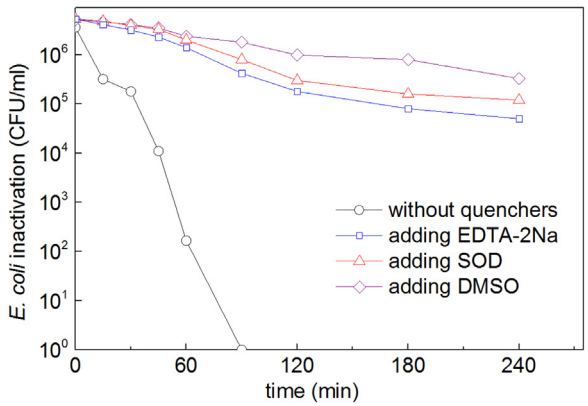

Fig. 8. *E. coli* inactivation on FeOx-TiO_2-PE film by itself and upon addition of ROS quenchers under solar simulated light (50 mW/cm^2).

3.5. Scavenging of oxidative radicals (ROS) during bacterial inactivation in aerobic media

Photocatalytic inactivation of bacteria in aerobic conditions proceeds by the highly oxidative radicals: OH°, HO_2°/O_2^- and cb (h^+). Fig. 8 presents the scavenging by dimethyl-sulfoxide (DMSO), superoxide dismutase (SOD) and

ethylene-tetra-acetic acid di-sodium salt (EDTA-2Na) to sort out the role of the OH°, O_2^- and TiO_2vb(h^+)/FeOxvb(h^+) respectively intervening in bacterial inactivation [5,9,18,39]. The TiO_2vb(h^+)/FeOxvb(h^+) valence holes seem to be the most efficient intermediate species leading to bacterial inactivation as shown in Fig. 8.

The OH°-radical would undergo the reduction OH°/OH^- when oxidizing bacteria (organic matter) with a potential of 1.9 eV vs NHE. The HO_2° radical at the pH of the bacterial inactivation shown in Fig. 6 (between 6 and 7) is present as $O_2^{-\circ}$, according to the reaction: $HO_2^\circ \leftrightarrow H^+ + O_2^{-\circ}$ (pka of 4.8). This photo-generated $O_2^{-\circ}$ have a potential of 0.75 eV vs NHE. Finally, the TiO_2(vbh+), being the most oxidizing species in the system, have a potential of 2.7 eV at pH 6. They would be the third species oxidizing the bacteria as shown in Fig. 8.

4. Conclusions

The effect of colloidal FeOx-TiO_2-PE films accelerating the bacterial inactivation was compared to TiO_2-PE and FeOx-PE films.

The FeOx-TiO_2-PE films release ppm amounts Fe during the repetitive recycling, but the film spectral absorption was not affected by the Fe-release. The induction of hydrophilicity in the FeOx-TiO_2-PE film during of the bacterial inactivation period favors the contact between *E. coli* and the film since *E. coli* presents a predominantly hydrophilic cell-wall envelope. Redox catalysis involving Fe- and Ti-species takes place during bacterial inactivation as reported by XPS experiments. The surface potential decreased during the period of bacterial inactivation due to the photo-induced damage on the cell-wall functional groups and mechanical integrity.

Acknowledgments

We thank the EPFL and the Swiss National Science Foundation (SNF) Project (200021-143283/1) for financial support. We also thank the COST Action 1106 for interactive discussions during the course of this study.

References

[1] H.A. Foster, I.B. Ditta, S. Varghese, A. Steele, Photo catalytic disinfection using titanium dioxide: spectrum and mechanism of antimicrobial activity, Appl. Microb. Biotechnol. 90 (2011) 1847–1868.
[2] J.-A. Byrne, P.S.M. Dunlop, J.H. Hamilton, P. Fernadez-Ibanes, I. Polo-Lopez, P. Kumar Sharma, A.S. Vennard, A review of heterogeneous photocatalysis for water disinfection, Molecules 20 (2015) 5574–5615.
[3] A. Kubacka, M. Suarez-Diez, D. Rojo, R. Bargiela, S. Ciordia, I. Zapico, J. Albar, C. Barbas, V. Martins dos Santos, M. Fernandez Garcia, M. Ferrer, Understanding the antimicrobial mechanism of TiO_2-based nanocomposite films in a pathogenic bacterium, Nat. Sci. Rep. 4 (2014) 4134–4139.
[4] K. Page, W. Wilson, I.P. Parkin, Antimicrobial surfaces and their potential in reducing the role of the inanimate environment in the incidence of hospital-acquired infections, J. Mater. Chem. 19 (2009) 3819–3831.
[5] M. Pelaez, N. Nolan, S.C. Pillai, M. Seery, Po Falaras, A. Kontos, M.S.P. Dunlop, J. Hamilton, J.-A. Byrne, K. O'Shea, M. Entezari, M. Entezari, D. Dionysiou, A review on the visible light active titanium dioxide photocatalsts for environmental applications, Appl. Catal. B 125 (2012) 331–345.
[6] R. Fagan, D. McCormack, D. Dionysiou, S.C. Pillai, A review of solar and visible light active TiO_2 photocatalysis for treating bacteria, cyanotoxins and contaminants of emerging concern, Mater. Sci. Semicond. Process. 42 (2016) 2–14.
[7] J. Podorska-Carroll, E. Panaitescu, B. Quilty, L. Wang, L. Menon, S.C. Pillai, Antimicrobial properties of highly efficient photocatalytic TiO_2 nanotubes, Appl. Catal. B 176-177 (2015) 70–75.
[8] S. Rtimi, C. Pulgarin, A. Houas, R. Sanjines, J.-C. Lavanchy, J. Kiwi, Coupling of narrow and wide band-gap semiconductors on uniform films in bacterial disinfection under low intensity visible light: implications of the interfacial charge transfer (IFTC), Hazard. Mater. 260 (2013) 860–868.
[9] J. Schneider, M. Matsuoka, M. Takeuchi, J. Zhang, Y. Horiuchi, M. Anpo, D. Bahnemann, Understanding TiO_2 photocatalysis: mechanisms and materials, Chem. Rev. 118 (2014) 9919–9986.
[10] M. Mishra, D. Chun, Alfa-Fe_2O_3 as a photocatalytic material: a review, Appl. Catal. A 498 (2015) 126–141.
[11] J. Kiwi, M. Graetzel, Light induced hydrogen formation and photo-uptake of oxygen in colloidal suspensions of alfa Fe_2O_3, J. Chem. Soc. Faraday Trans. 1 (1987) 1101–1108.
[12] W. Zhou, H. Fu, K. Pan, C. Tian, Y. Qu, Mesoporous TiO_2/α-Fe_2O_3: bifunctional composites for effective elimination of arsenite contamination through simultaneous photocatalytic oxidation and adsorption, J. Phys. Chem. C 112 (2008) 19584–19592.
[13] Y. Cong, Z. Li, Y. Zhang, Q. Wang, Q. Xu, Synthesis of-Fe_2O_3/TiO_2 nanotube arrays for photoelectro-Fenton degradation of phenol, Chem. Eng. J. 191 (2012) 356–363.
[14] B. Palanisamy, C. Babu, B. Sundarevel, S. Anandan, V. Murugesan, Sol–gel synthesys of mesoporous mixed Fe_2O_3/TiO_2 photocatalyst: application for degradation of 4-chlorophenol, J. Hazard. Mater. 252 (2013) 233–242.
[15] Q. Zhang, G. Rao, J. Rogers, C. Zhao, L. Liu, Y. Li, Novel anti-fouling Fe_2O_3/TiO_2 nanowire membranes for humic acid removal from water, Chem. Eng. J. 271 (2015) 180–187.
[16] S. Rtimi, C. Pulgarin, R. Sanjines, J. Kiwi, Novel FeOx-polyethylene (PE) transparent films: synthesis and mechanism of surface regeneration, RSC Adv. 5 (2015) 80203–80211.
[17] S. Rtimi, R. Sanjines, J. Kiwi, C. Pulgarin, M. Bensimon, I. Kmehl, V. Nadtochenko, Innovative photocatalyst (FeOx-TiO_2): transients induced by Femtosecond laser leading to bacterial inactivation under visible light, RSC Adv. 5 (2015) 101751–101759.
[18] A. Fujishima, X. Zhang, D. Tryck, TiO_2 photocatalysis and related surface phenomena, Surf. Sci. Rep. 63 (2008) 515–546.
[19] M. Mohaptra, S. Anand, Synthesis and applications of nanostructured iron oxides/hydroxides—a review, Int. J. Sci. Technol. 2 (2010) 127–146.
[20] M. Dhananjeyan, E. Mielczarski, K. Thampi, Ph. Buffat, M. Bensimon, A. Kulik, J. Mielczarski, J. Kiwi, Photodynamics and surface characterization of immobilized TiO_2 and Fe_2O_3 photo-catalysts on modified polyethylene films, J. Phys. Chem. B 105 (2000) 12046–12055.
[21] J. Fernandez, J. Bandara, A. Lopez, Ph. Buffat, J. Kiwi, Photo-assisted fenton degradation of non-biodegradable azo-dye (Orange II) in Fe-free solutions mediated by cation transfer membranes, Langmuir 15 (1999) 185–192.
[22] S. Rtimi, R. Sanjines, M. Andrzejczuk, C. Pulgarin, A. Kulik, J. Kiwi, Innovative transparent non-scattering TiO2 bactericide thin films inducing increased E. coli cell wall fluidity, Surf. Caot Technol. 254 (2014) 333–343.
[23] S. Rtimi, C. Pulgarin, R. Sanjines, J. Kiwi, Innovative semi-transparent nano-composite films presenting photo-switchable behavior and leading to a reduction of the risk of infection under sunlight 3 (2013) 16345-16348.
[24] L.L. Stookey, Ferrozine, a new spectrophotometric reagent for iron, Anal. Chem. 42 (1970) 779–781.
[25] C. Wagner, W. Riggs, L. Davis, G. Mullenberg (Eds.), Handbook of X-ray Photoelectron Spectroscopy, Perkin-Elmer Corporation Physical Electronics Division, Minnesota, USA, 1979.
[26] J. Nogier, M. Delamar, P. Ruiz, M. Gratzel, R. Thampi, J. Kiwi, X-ray photoelectron spectroscopy of V_2O_5/TiO_2 catalysts, Catal. Today 20 (1994) 109–119.
[27] P. Wardman, Reduction potentials of one electron couples involving free radicals in aqueous solutions, J. Phys. Chem. Ref. Data 18 (1989) 1637–1755.
[28] International Organization for Standardization: Water quality determination of iron, Geneva, 1988 (ISO 6332:1988), Guidelines for drinking-water quality, 2nd ed. Vol. 2: Health criteria and supporting information, World Health Organization Geneva, 1996.
[29] K. Hardee, A. Bard, Photochemical behavior of several polycrystalline oxides electrodes in aqueous solutions, J. Electrochem. Soc. 124 (1977) 215–224.
[30] N. Sakai, A. Fujishima, T. Watanabe, K. Hashimoto, Enhancement of the photo induced hydrophilic conversion rate of TiO_2 film electrode surfacesby anodic polarization, J. Phys. Chem. Chem. B 105 (2001) 3023–3026.
[31] K. Hashimoto, I. Hirie, A. Fujishima, TiO_2 photocatalysis: an overview and furure prospects, AAPPS Bull 17 (2005) 12–28.
[32] C. Gunawan, W. Teoh, P. Marquis, J. Lifla, R. Amal, Reversible antimicrobial photoswitching nanosilver, Small 5 (2009) 341–344.
[33] M. van Loosdrecht, J. Lyklema, W. Norde, G. Schraa, A. Zehnder, The role of Bacterial cell-wall hydrophobicity in adhesiaon, Appl. Environ. Microb. 53 (1987) 1001–1893.
[34] A.D. Shirley, Corrections for electrostatic charged species in XPS-spectroscopy, Phys. Rev. B5 (1987) 4709–4716.
[35] V. Nadtochenko, J. Kiwi, Photolysis of $FeOH^{2+}$ and $FeCl^{2+}$ in aqueous solution: photo-dissociation kinetics and quantum yields, Inorg. Chem. 37 (1998) 5233.
[36] A. Kraeutler, A. Bard, J. Am. Chem. Soc. 1100 (1978) 239–2244.
[37] Z. Lu, L. Zhou, Z. Zhang, W. Shi, Z. Xie, H. Xie, D. Pang, P. Shen, Cell damage induced by photocatalysis in TiO_2Thin films, Langmuir 19 (2003) 8765–8768.
[38] J.G. Fitz, T.E. Trouuillot, B.F. Scharschmidt, Effect of pH on membrane potential and K^+ conductance in cultured rat hepatocytes, Gastro Liver Phys. 257 (1989) G961–G968.
[39] J. Kiwi, V. Nadtochenko, New evidence for TiO_2 photocatalysis during bilayer lipid peroxidation, J. Phys. Chem. B 109 (1994) 17675–17684.
[40] S. Leytner, J.T. Hupp, Evaluation of the energetics of electron trap states at the nanocrystalline titanium dioxide/aqueous solution interface via time-resolved photo-acoustic spectroscopy, Chem. Phys. Lett. 330 (2000) 231–2237.
[41] D.C. Hurum, A.G. Agrios, K.A. Gray, T. Rajh, M.C. Thurnauer, Explaining the enhanced photocatalytic activity of degussa P25 mixed-Phase TiO_2 using EPR, J. Phys. Chem. B 107 (2003) 4545–45490.